Micromechanical crack growth-based fatigue damage in fibrous composites

Dear Author,

Please, note that changes made to the HTML content will be added to the article before publication, but are not reflected in this PDF.

Note also that this file should not be used for submitting corrections.

International Journal of Fatigue xxx (2015) xxx–xxx

Contents lists available at ScienceDirect

International Journal of Fatigue

journal homepage: www.elsevier.com/locate/ijfatigue

Micromechanical crack growth-based fatigue damage in fibrous composites

Roberto Brighenti *, Andrea Carpinteri, Daniela Scorza

Dept. of Civil-Environmental Engng & Architecture, Univ. of Parma, 43100 Parma, Italy

ARTICLE INFO

Article history:
Received 21 October 2014
Received in revised form 6 April 2015
Accepted 10 April 2015
Available online xxxx

Keywords:
Fibre-reinforced composites
Fatigue
Debonding
Damage
Crack growth

ABSTRACT

A partially debonded fibre can be analysed as a 3-D mixed Mode fracture case, for which the fibre–matrix detachment growth – leading to a progressive loss of the composite's bearing capacity – can be assessed through classical fatigue crack propagation laws. In the present research, the above mentioned case is firstly examined from the fracture mechanics theoretical point of view, and the effects of the stress field in the matrix material on the Stress Intensity Factors – SIFs – (associated to the crack representing the fibre–matrix detachment) are taken into account. Fatigue effects on the matrix material are accounted for by means of a mechanical damage, quantified through a Wöhler-based approach. A damage scalar parameter aimed at measuring the debonding severity during fatigue process is also introduced. Finally, some numerical simulations are performed, and the obtained results are compared with experimental data found in the literature.

1. Introduction

Composite structural materials typically consist of two or more constituents combined at a macroscopic level. Their classification is usually based on the kind of matrix material (polymers, metals, ceramics) and of reinforcing phase (fibres, particles, flakes). Due to their high-quality mechanical properties (such as improved tensile strength, fracture resistance, durability, corrosion resistance, enhanced wear and fatigue strength), composite materials – such as the fibre-reinforced ones – are commonly used in advanced engineering applications where traditional materials cannot conveniently be employed [1–3]. The mechanical properties of such multiphase materials depend on those of their constituents, i.e. the bulk material (matrix) and the reinforcing phase (such as fibres), as well as on their reciprocal interface bonding.

The strength and durability design of composite structural components must consider the typical damage phenomena occurring in such materials under in-service loading. Such degrading effects, typically responsible for a significant decrease of the mechanical performances of the structures, can mainly be related to the fibre–matrix delamination (also identified as debonding), fibre breaking, fibre buckling, matrix plastic deformation or cracking. These effects can be particularly relevant and dangerous for structural components under repeated loading [4–6].

The present research deals with a micromechanical-based approach for examining the fatigue behaviour of short-fibre-reinforced composites under uniaxial cyclic loading. The assessments of the damaging effects occurring in such non-homogeneous materials subjected to uniaxial cyclic loading (even under load levels much below the material strength) are very complex. Simple and reliable mechanics-based models for quantitative evaluation of such damaging effects are needed. In particular, the main degrading effects taking place in the matrix, in the fibres and affecting their reciprocal bonding are herein taken into account and quantified by analysing the mechanical damaging phenomena occurring at the micro-scale level.

The last Sections of the present paper show some comparisons with experimental data, and discuss some results of a parametric simulation aimed at underlying the mechanical effects of the involved parameters on the fatigue behaviour of fibre-reinforced multiphase materials.

2. Mechanics of fibre–matrix detachment

2.1. Shear lag model

At the beginning of the composite science development, the fibre–matrix debonding was studied through the classical shear lag model initially proposed by Cox [7]. Such a model examines a cylindrical portion of composite made by a fibre surrounded by a sufficiently large volume of matrix material, under remote tensile

* Corresponding author.
E-mail address: brigh@unipr.it (R. Brighenti).

http://dx.doi.org/10.1016/j.ijfatigue.2015.04.007
0142-1123/

Nomenclature

$A, B > 0$ Wöhler's fatigue constants of the matrix material
c Fibre perimeter
C_i, m_i Paris constants of the fibre–matrix interface
$D_c(\sigma^*, R^*, N)$ Damage parameter after N loading cycles with stress amplitude σ^* and stress ratio R^*
$D_i = l/L_f$ Fibre debonding-related damage parameter
E_i Fibre–matrix interface Young modulus
$E_{m0}, E_m(N)$ Young modulus for the undamaged matrix material and reduced Young modulus after N loading cycles
E_f Elastic modulus of the fibre
$\mathcal{G}_{ic}$ Fibre–matrix interface fracture energy
$\bar{k}$ Shear stiffness of the fibre–matrix bonding
K_i Equivalent SIF for a partially debonded fibre
$K_{IC}, \Delta K_{th}$ Fibre–matrix interface fracture toughness and threshold SIF, respectively
$K_I(\sigma_r^\infty), K_{II}(\sigma_r^\infty) K_{II}(\sigma_z^\infty), K_{Mw}^*$ Mode I and Mode II SIFs due to the remote stresses σ_r^∞ and σ_z^∞ , respectively, and dimensionless SIFs due to the remote stress σ_w^∞ $(w = r, z)$
ΔK_i Stress-Intensity Factor range at the fibre–matrix interface
$L_{ad}, L_f, l = L_f - L_{ad}$ Adhesion length of a partially debonded fibre, fibre semi-length, and fibre debonded length, respectively
N^* Number of loading cycles to failure under stress amplitude $\sigma^* \leqslant \sigma_0$
$R = \sigma_{\min}/\sigma_{\max}$ Load ratio of the constant amplitude stress cycles
$v_{cg} = dl/dN$ Crack growth velocity measured with respect to the number of loading cycles
$\alpha = \frac{1}{(E_m \cdot A_m)} + \frac{1}{(E_f \cdot A_f)} \beta = \sqrt{c \cdot \bar{k} \cdot \alpha}$ Parameters of the fibre–matrix composite material
$\varepsilon_f(z), \varepsilon_f^m, \overline{\varepsilon_f^m}$ Fibre strain and matrix strain measured along the fibre direction, and mean value of matrix strain
$[[\varepsilon_{f-m}(z)]], [[\overline{\varepsilon_{f-m}}]]$ Difference between the matrix and the fibre strain (strain jump) and corresponding averaged value along the fibre, respectively
v_i, ϕ_f Fibre–matrix interface Poisson's ratio, and diameter of the fibre
μ, η Fibre volume fraction and matrix volume fraction
σ^*, σ_0^* Generic stress amplitude, and conventional fatigue limit of the matrix material
$\sigma_z^m(z), \sigma_z^f(z)$ Stress in the matrix material and in the fibre acting along the z-axis (coincident with the fibre direction)
$\sigma_r^\infty, \sigma_z^\infty$ Remote radial stress and remote axial stress (acting on a fibre)
$\tau_f(z)$ Fibre–matrix interface shear stress
$\tau_{f,f}, \tau_{f,u}$ Interface friction stress, and ultimate adhesion fibre–matrix interface shear stress

stress acting parallel to the fibre direction (Fig. 1a). The corresponding fibre–matrix interface shear stress $\tau_f(z)$ and the normal stress $\sigma_z^m(z)$ (acting parallel to the fibre axis) in the matrix can be expressed as follows (Fig. 1a) [8,9]:

$$\tau_f(z) = \frac{F \cdot \beta}{c} \cdot \left[\frac{\sinh(\beta \cdot z)}{\cosh(\beta \cdot L_f)}\right]$$

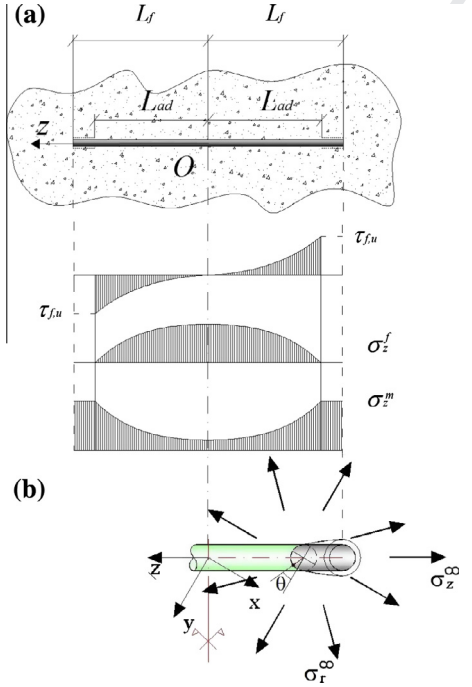

Fig. 1. (a) Stress distributions along the fibre in a partial debonding stage; (b) debonded extremity (3D cylindrical crack) of a fibre under remote radial (σ_r^∞) and axial (σ_z^∞) stresses.

$$\sigma_z^m(z) = \frac{P - f(z)}{A_m} = \frac{F}{A_m} \cdot \left\{\alpha \cdot E_m \cdot A_m - \left[1 - \frac{\cosh(\beta \cdot z)}{\cosh(\beta \cdot L_f)}\right]\right\} \quad (1)$$

with $\sigma_z^f(z) \cdot A_f + \sigma_z^m(z) \cdot A_m = P$

where P is the total force sustained by the composite cylindrical element, c is the fibre perimeter, A_f and A_m are the cross section of the fibre and of the matrix that surrounds the single fibre, respectively, and $f(z) = \sigma_z^f(z) \cdot A_f$ is the axial force in the fibre.

Further:

$$\alpha = (E_m \cdot A_m)^{-1} + (E_f \cdot A_f)^{-1}, \ \beta = \sqrt{c \cdot \bar{k} \cdot \alpha}, \ F = P/(\alpha \cdot E_m \cdot A_m) \quad (1a)$$

where $\bar{k}$ is the stiffness of the fibre–matrix interface.

The strain jump, $[[\varepsilon_{f\text{-}m}(z)]]$, i.e. the difference between the matrix strain and the fibre strain, occurring in correspondence of the detached zones, can be written as follows [8,9]:

$$[[\varepsilon_{f-m}(z)]] = \varepsilon_f^m(z) - \varepsilon_f(z) \quad \text{with } \varepsilon_f(z) = s(\varepsilon_f^m(z)) \cdot \varepsilon_f^m(z) \quad (2)$$

where $s(z)$ is a scalar function which quantifies the local 'degree of sliding' between the fibre and the matrix. When $s(z) = 0$, the detachment is complete and $[[\varepsilon_{f-m}(z)]] = \varepsilon_f^m(z)$. When the bond is perfect – i.e. no strain jump occurs $[[\varepsilon_{f\text{-}m}(z)]] = 0$ – the sliding function tends to the unity, and the fibre strain coincides with the matrix strain in the fibre direction, $\varepsilon_f^m(z)$. Such a function can conveniently be written by using average quantities:

$$[[\overline{\varepsilon_{f-m}}]] = \overline{\varepsilon_f^m} - \varepsilon_f = \overline{\varepsilon_f^m} \cdot \left[1 - s(\overline{\varepsilon_f^m})\right] \quad (2a)$$

Consequently its mean value, $s(\overline{\varepsilon_f^m})$, can be evaluated based on the energy equivalence, i.e. by equating the actual elastic energy W stored in the fibre with the average energy $\bar{W}$ [4]:

$$s(\overline{\varepsilon_f^m}) = \frac{1}{\overline{\varepsilon_f^m} \cdot E_f} \cdot \sqrt{\frac{\int_{-L_f}^{L_f} \sigma_z^{f^2}(z) dz}{2L_f}} \quad (3)$$

where $\overline{\varepsilon_f^m} = \frac{1}{2L_f} \cdot \int_{-L_f}^{L_f} \varepsilon_f^m(z)dz$ and $\sigma_z^f(z) = f(z)/A_f$.

Since the reinforcing fibres are assumed to have a linear elastic behaviour, the above energy, W, must be evaluated according to the effective axial stress distribution in the fibre, whereas the corresponding average quantity, $\bar{W}$, can be determined by considering an equivalent constant stress distribution, $\overline{\sigma_z^f}$, along the fibre.

According to the shear lag approach, the debonding phenomenon proceeds when the maximum value of the interface shear stress is attained at the extremities (Fig. 1a) of the actual adhesion length $z(z = L_f$ for a complete bonded fibre and $z = L_{ad}$ for a partially debonded fibre). In such a situation, the previous Eqs. (1), (1a), (2), (2a), (3) are still valid as long as the fibre semi-length, L_f, is replaced with the half of the total bonded length, L_{ad}. The critical condition for the fibre detachment extension can be written as follows [8]:

$$\tau_{f,\max} = \tau_f(z = L_{ad}) = \frac{F \cdot \beta}{c} \cdot \tanh(\beta \cdot L_{ad}) \cong \sigma_z^\infty \cdot \frac{\beta}{c \cdot (\alpha \cdot E_m)} \cdot \tanh(\beta \cdot L_{ad}) = \tau_{f,u} \tag{4a}$$

$$\Rightarrow \quad \sigma_{z,c}^\infty \geqslant \frac{\tau_{f,u} \cdot c \cdot \alpha \cdot E_m}{\beta \cdot \tanh(\beta \cdot L_{ad})} \tag{4b}$$

where $\tau_{f,u}$ is the ultimate adhesion fibre–matrix interface shear stress for the involved materials.

Along the fibre debonded length zones (Fig. 1a), $l = L_f - L_{ad}$, the shear stress arising at the interface can be assumed to be equal to the friction shear stress $\tau_{f,f}$. However, such a residual shear strength (depending also on the radial stress acting on the fibre) can reasonably be neglected, as is done in the following, because its contribution to the composite bearing capacity is generally very limited.

2.2. Fracture mechanics approach

The problem of an elastic bi-material plane with an interface crack has widely been studied [10–12]. The extension of such a problem to a 3D case can conveniently be used to describe the detachment phenomenon in short-fibre-reinforced materials through fracture mechanics concepts.

Since the fibres are assumed to have a cylindrical shape, the three-dimensional crack arising in a partially debonded fibre can be analysed by considering the debonded zone as a 3D cylindrical crack lying between two different materials [13–15].

By taking into account the generic case of a fibre embedded in an elastic matrix (Fig. 1b) under remote axial (σ_z^∞) and radial (σ_r^∞) stresses, the energetically equivalent SIF, along the circular crack front, can be defined as follows [16,17]:

$$K_i = \begin{cases} \sqrt{K_I^2(\sigma_r^\infty) + [K_{II}(\sigma_r^\infty) + K_{II}(\sigma_z^\infty)]^2} & \sigma_r^\infty > 0 \\ K_{II}(\sigma_z^\infty) & \sigma_r^\infty \leqslant 0 \end{cases} \quad \text{with } K_{Mw}^* = \frac{K_M(\sigma_w^\infty)}{\sigma_w^\infty \sqrt{\pi l}} \tag{5}$$

where $K_{Mw} = K_M(\sigma_w^\infty)$ indicates the generic Mode M SIF (M = I, II) due to the remote stress σ_w^∞ ($w = r, z$), and K^*_{Mw} is the corresponding dimensionless value. Note that all the above SIFs, $K_i, K_I(\sigma_r^\infty)$, $K_{II}(\sigma_r^\infty), K_{II}(\sigma_z^\infty)$, are independent of the angular co-ordinate θ due to the axial symmetry of the problem.

As a representative example of the fracture mechanics problem under study, the dimensionless Mode II SIFs, K^*_{IIz} and K^*_{IIr}, due to remote longitudinal (σ_z^∞) and radial (σ_r^∞) stress, are plotted in Fig. 2 for different values of the Young modulus ratio, E_f/E_m. As can be noted, the SIFs are increasing functions of the modulus ratio, while the SIF values decreases by increasing the aspect ratio of the fibre, $2 \cdot L_f/\phi_f$, i.e. the SIFs are much more severe for short fibre–matrix detached length.

In first approximation, the remote axial stress produces only a Mode II SIF, whereas the remote positive radial stress is mainly responsible for both Mode I and Mode II SIFs. The last cited stress-intensity factor arises due to the different elastic properties of the two joined materials.

The equivalent SIF at the fibre–matrix interface crack front (see Eq. (4)) can be used to define the condition of unstable crack propagation, according to the Griffith's energy-based approach:

$$K_i = K_{ic} = \begin{cases} \sqrt{E_i \cdot \mathcal{G}_{ic}} & \text{plane stress} \\ \sqrt{\frac{E_i \cdot \mathcal{G}_{ic}}{1 - \nu_i^2}} & \text{plane strain} \end{cases} \tag{6}$$

where $\mathcal{G}_{ic}$ is the critical interface fracture energy, K_{ic} is the corresponding fracture toughness, and E_i and ν_i are the Young modulus and the Poisson ratio at the interface, respectively [18].

In order to find out a relationship between the shear lag model and the fracture approach, the above critical condition (Eq. (6)) can be examined in the particular case of a simply axial remote stress σ_z^∞ only. The following expression can be written:

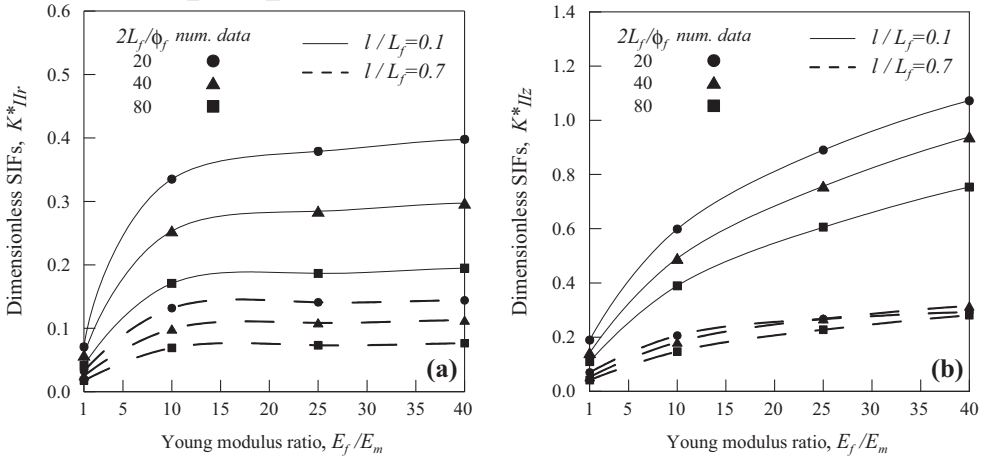

Fig. 2. Dimensionless radial and longitudinal Mode II SIF, $K_{II,r}$ (a) and $K_{II,z}$ (b), vs Young modulus ratio, E_f/E_m, for different values of fibre aspect ratio, $2 \cdot L_f/\phi_f$, and relative debonded length equal to 0.1 and 0.7.

Please cite this article in press as: Brighenti R et al. Micromechanical crack growth-based fatigue damage in fibrous composites. Int J Fatigue (2015), http://dx.doi.org/10.1016/j.ijfatigue.2015.04.007

$$K_i = K_{IIz} = K_{II}(\sigma_z^\infty) = K_{IIz}^* \cdot \sigma_z^\infty \sqrt{\pi l} \rightarrow \sigma_{z,c}^\infty \geqslant \frac{\sqrt{E_i \cdot \mathcal{G}_{ic}}}{K_{IIz}^* \cdot \sqrt{\pi l}} \tag{7}$$

By equating the above critical conditions in Eqs. (4b) and (7), both expressed in terms of remote critical axial stress $\sigma_{z,c}^\infty$, the analytical relationship between the ultimate adhesion fibre–matrix interface shear stress $\tau_{f,u}$ and the fibre–matrix interface fracture toughness K_{ic} (or equivalently the interface fracture energy $\mathcal{G}_{ic}$) can be obtained once the dimensionless SIF, $K_{IIz}^*(l = L_f - L_{ad})$, is known for a given fibre detached length ($l = L_f - L_{ad}$).

As is mentioned above, this comparison is restricted to the case of remote stresses acting in the fibre direction, which corresponds to the only case admitted by the shear lag model. In real cases, even if the loading condition is purely uniaxial, the stress state at the fibre–matrix interface is more complex (generally, it is not uniaxial due to the generic fibre orientation) and, therefore, the problem cannot be tackled and solved by using the classical shear lag theory, whereas it can easily be treated through fracture mechanics. The existence of stresses σ_r^∞ transversal to the fibre could be taken into account in the shear lag theory by replacing the ultimate fibre–matrix interface shear stress $\tau_{f,u}$ with $\tau_{f,u}(\sigma_r^\infty)$. In other words, by adopting the shear lag approach, the remote radial stress can be accounted for through its effect on the ultimate shear stress: a tensile radial stress can reasonably be considered to be responsible for a reduction of such a limit shear stress.

Consequently, as is mentioned above, the critical conditions can be determined by combining Eq. (4a) and Eq. (7):

$$K_{ic} = \tau_{f,u}(\sigma_r^\infty) \cdot \left[\frac{c \cdot \alpha \cdot E_m}{\beta \cdot \tanh(\beta \cdot L_{ad})}\right] \cdot \left[\sqrt{a^2 \cdot K_{Ir}^{*2} + (a \cdot K_{IIr}^* + K_{IIz})^{*2}} \cdot \sqrt{\pi l}\right] \tag{8a}$$

or

$$\mathcal{G}_{ic} = \tau_{f,u}^2(\sigma_r^\infty) \cdot \left[\frac{c \cdot \alpha \cdot E_m}{\beta \cdot \tanh(\beta \cdot L_{ad})}\right]^2 \cdot \frac{\left[a^2 \cdot K_{Ir}^{*2} + (a \cdot K_{IIr}^* + K_{IIz}^*)^2\right] \cdot \pi l}{E_i} \tag{8b}$$

where E_i is the elastic modulus of the fibre–matrix interface, and the remote radial stress is assumed to be expressed as $\sigma_r^\infty = a \cdot \sigma_z^\infty$, with a being a constant.

Since the interface fracture toughness K_{ic} is a characteristic value of the joined materials, the limit interface shear stress under the remote radial stress value, $\tau_{f,u}(\sigma_r^\infty)$, can be obtained from Eq. (8a), and expressed through the following form:

$$\tau_{f,u}(\sigma_r^\infty) = \tau_{f,u} \cdot M(\sigma_r^\infty) \tag{9}$$

$$\tau_{f,u}(\sigma_r^\infty) = \tau_{f,u} \cdot \frac{\overbrace{K_{IIz}^*}^{M(\sigma_r^\infty)}}{\sqrt{a^2 \cdot K_{Ir}^{*2} + (a \cdot K_{IIr}^* + K_{IIz})^{*2}}}$$

where $\tau_{f,u}$ must be considered as the limit shear stress in the case of no radial stress.

In other words, the knowledge of the dimensionless SIFs in Eq. (9) allows us to define the ultimate fibre–matrix shear stress in presence of a tensile remote radial stress. In practical cases, Eq. (8) can be used to evaluate the fibre–matrix interface fracture energy $\mathcal{G}_{ic}$ (or the corresponding fracture toughness K_{ic}), once the ultimate shear strength $\tau_{f,u}$ is known.

As is shown in the following sections, such a fracture mechanics approach for the assessment of the debonding phenomenon gives us the possibility to determine the progressive fibre matrix detachment (during fatigue loading) by using classical crack growth-rate equations, typically employed to evaluate the stable crack propagation produced by repeated loadings on structural components.

3. Mechanical model of fibre-reinforced composite under cyclic loading

The mechanical behaviour of fibre-reinforced materials under cyclic loading is a complex issue because several damage phenomena occur in the composite material, such as the matrix degradation, the reduction of the mechanical properties of the fibres and the fibre–matrix interface.

In the present research, the damage occurring in the matrix and that at the fibre–matrix interface are considered as non interacting phenomena, i.e. each of such damages can be assessed independent of the other one. For the sake of simplicity, we assume that the degrading effect of the cyclic loading on the mechanical properties of the fibre material is completely neglected since, in the case of short-fibre reinforced composites characterised by fibres elastic modulus much greater than that of the surrounding matrix and a weak interface, this contribution is less significant than the two contributions mentioned above. The fatigue effect on the fibres is usually responsible for fibre breaking [19] occurring after a proper number of loading cycles, whereas their load carrying capacity can be assumed to remain practically unchanged up to the achievement of their failure condition.

Concerning the matrix damage, the hypothesis of no crack formation and propagation in the bulk material is adopted, since the case of ductile matrix is considered.

3.1. Fatigue effects on the interface fibre–matrix detachment and matrix damage

As is well-known, the cyclic loading reduces the mechanical properties of materials due to the irreversible rearrangement of the lattice structure at the microscopic level.

In composite materials, the repeated loadings are responsible for the decrease of the matrix mechanical properties and for the reduction of the fibre–matrix bond effectiveness.

As is mentioned above, the progressive fibre–matrix debonding can be quantified through exponential fatigue propagation laws, applied to the crack representing the discontinuity at the detached ends of the fibres.

The crack propagation assessment can be performed through the debonding length rate law, or the crack growth velocity v_{cg} quantified with respect to the number of loading cycles, defined by the classical Paris law:

$$v_{cg} = dl/dN = C_i \cdot \Delta K_i^{m_i}, \qquad \Delta K_{th} < \Delta K_i \leqslant K_{IC} \tag{10}$$

where C_i, m_i are the Paris constants of the interface, l is the debonded length (Fig. 1) and ΔK_i is the equivalent stress intensity factor range produced by the cyclic remote stresses. For the sake of simplicity, the far field cyclic stresses are assumed to vary according to constant-amplitude in-phase cycles, in order to be able to define an equivalent cyclic SIF range.

The above relationship can be used to determine the critical detached length and the number of loading cycles N_c necessary to get such a critical condition under repeated loading:

$$l(N_c) = l_c = \int_0^{N_c} C_i \cdot \Delta K_i^{m_i} dN, \quad \text{such that } \Delta K_i(l_c, \sigma_z^\infty, \sigma_r^\infty) = K_{IC} \tag{11a}$$

$$D_i(N) = l(N)/l_c \geqslant 0 \tag{11b}$$

where the interface equivalent SIF range (see Eq. (5)), $\Delta K_i(l, \sigma_z^\infty, \sigma_r^\infty)$ depends on the remote stress field and on the current debonded

length for the given composite material. According to such a relationship, a debonding-related damage D_i (Eq. (11b)) can also be defined as the ratio between the current debonded length $l(N_c)$ and the critical one l_c [20]. The debonded critical length corresponds to the condition of unstable crack propagation, that is, the condition of complete fibre detachment from the matrix material for which the damage is complete, i.e. $D_i(N_c) = 1$.

On the other hand, it is shown below that $K_i(l, \sigma_z^\infty, \sigma_r^\infty)$ is a decreasing function of l. Therefore, the SIF decreases as the detached length increases, implying that the critical condition (Eq. (11a)) cannot be reached during crack propagation. In this case, the debonding-related damage D_i can more conveniently be defined as follows:

$$0 \leqslant D_i = l/L_f \leqslant 1 \tag{12}$$

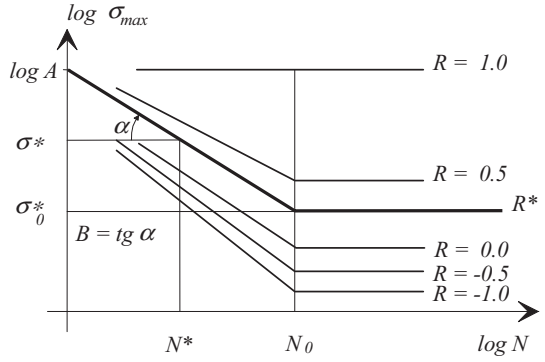

Fig. 3. Example of Wöhler's curves for different values of stress ratio R.

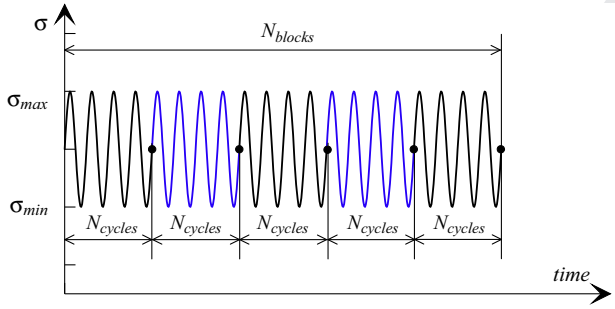

Fig. 4. Constant amplitude stress cycles subdivided in N_{blocks} with N_{cycles} for each block.

Such a degrading parameter referred to the interface region quantitatively describes the effectiveness of the fibre in the bearing mechanism of the composite material.

On the other hand, according to the shear lag model, the detachment phenomenon can synthetically be quantified also through the sliding function $s(\overline{\varepsilon_f^m})$ (Eq. (2)), and the interface damage can thus be measured as $D_i = 1 - s(\overline{\varepsilon_f^m})$ from which, by taking into account Eq. (12), the scalar function $s(\overline{\varepsilon_f^m})$ can approximately be estimated as follows: $s(\overline{\varepsilon_f^m}) = (L_f - l)/L_f$.

Let us consider now the fatigue effects on the matrix material. The degradation produced by uniaxial constant amplitude cyclic loads on a homogeneous material can be evaluated through the so-called S–N curves (Fig. 3), also known as Wöhler curves, that define the cyclic loading range to failure against the number of loading cycles for a given value of stress ratio $R = \sigma_{min}/\sigma_{max}$ (under the hypothesis of high-cycle fatigue regime).

Such curves can empirically be approximated by the following relationships:

$$N = \begin{cases} \left(\frac{\sigma}{A}\right)^{-\frac{1}{B}} = \text{const} \cdot \sigma^{-\frac{1}{B}}, & \sigma > \sigma_0 \\ \infty & \sigma \leqslant \sigma_0 \end{cases} \tag{13}$$

where A, $B > 0$ are fatigue constants of the material, and σ_0^* is the apparent fatigue limit of the material under cyclic stress characterized by stress ratio equal to R^*. In the case of uniaxial stress state, the number N^* of loading cycles to failure can be written as follows:

$$N^* = A^{1/B}\sigma^{*-1/B}$$

A reasonable damage parameter D_c to quantify the damage accumulation can be the following one:

$$\begin{cases} D_c(\sigma^*, R^*, N) = \frac{N}{N^*} = \frac{N}{(\sigma^*/A)^{-1/B}} < 1 & \text{if } \sigma^* > \sigma_0 \\ D_c(\sigma^*, R^*, N) = 0 \quad \forall N & \text{if } \sigma^* \leqslant \sigma_0 \end{cases} \tag{14}$$

where D_c is defined by the ratio between the current number of loading cycles N, for given values of stress amplitude and stress ratio, and the corresponding number of loading cycles, N^*, to failure for the same remote stress parameters.

In the case of cyclic loads characterized by $\sigma^* \leqslant \sigma_0$, the damage is assumed to be equal to zero, while the failure condition (fully damaged material) is reached when the damage parameter is equal to 1, $D_c(\sigma^*, R^*, N) = 1$.

This approach can also be interpreted as the way to update the mechanical properties of the matrix, reduced by the damaging effect of the progressive fatigue loading [4]. The above assessment can be carried out according to the following relationship:

$$P_m(N) = P_{m,0} \cdot [1 - D_c(\sigma^*, R^*, N)] \tag{15}$$

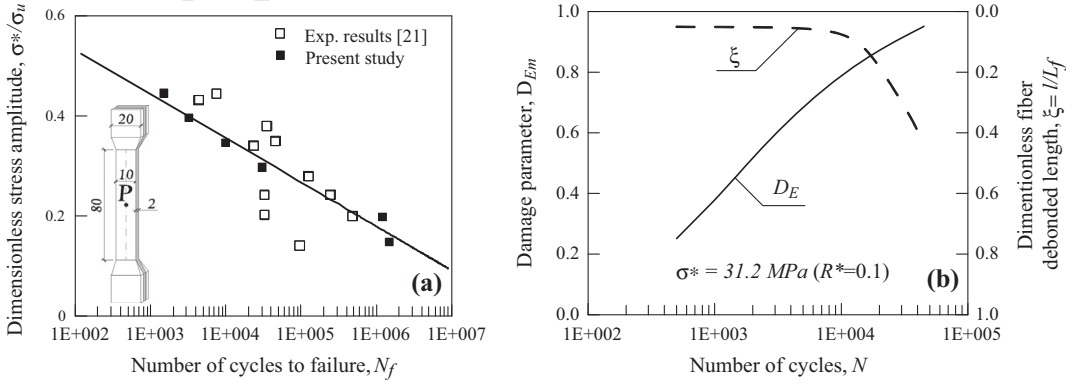

Fig. 5. (a) Wöhler's curves for a glass fibre-reinforced polycarbonate specimen (dimensions in mm): experimental and present results. (b) Damage evolution in the matrix and dimensionless debonding in the fibres (at point P) vs the number of stress cycles.

Please cite this article in press as: Brighenti R et al. Micromechanical crack growth-based fatigue damage in fibrous composites. Int J Fatigue (2015), http://dx.doi.org/10.1016/j.ijfatigue.2015.04.007

where P_{m0} is an undamaged generic mechanical parameter of the material, and P_m is the corresponding damaged one. The above reduction is written through the damage parameter D_c which is assumed to be expressed in the form of Eq. (14), i.e. as piecewise linear function of the number of loading cycles. In the case of multiaxial stress states, the previous equations can be applied by replacing σ^* with the combined stress σ_{eq} related to the yielding or failure criteria of the matrix material being examined. Alternatively, the principal stress amplitude can be adopted.

An advisable choice is to impose $P_{m0} = E_{m0}$, where E_{m0} is the undamaged Young modulus of the matrix material. The damaged corresponding counterpart is the damaged Young modulus $E_m(N)$:

$$E_m(N) = E_{m0} \cdot [1 - D_{cm}(\sigma^*, R^*, N)] \tag{16}$$

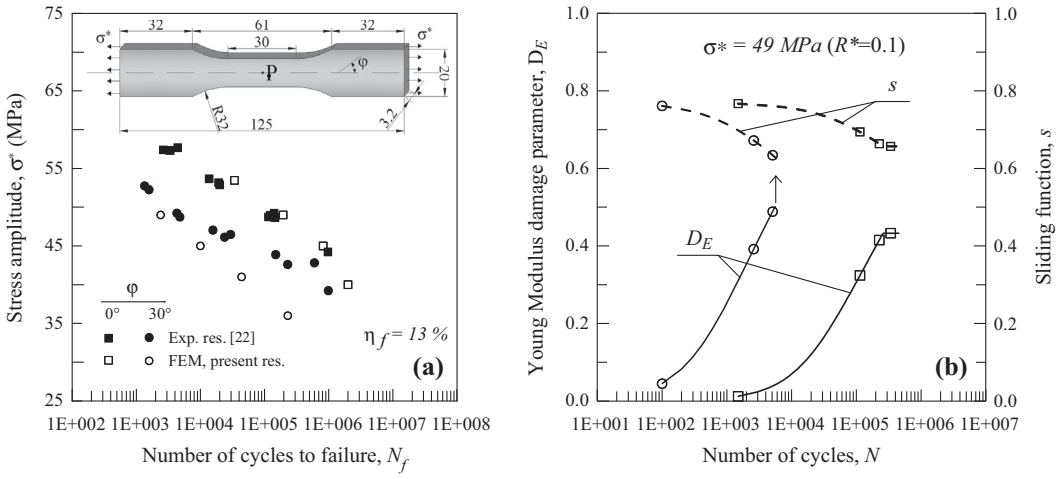

Fig. 6. (a) Wöhler's curves for a glass fibre-reinforced polyamide (sizes in mm) with two different fibre orientations: experimental and present FEM results. (b) Damage evolution in the matrix and fibres sliding parameter (at point P) vs the number of stress cycles.

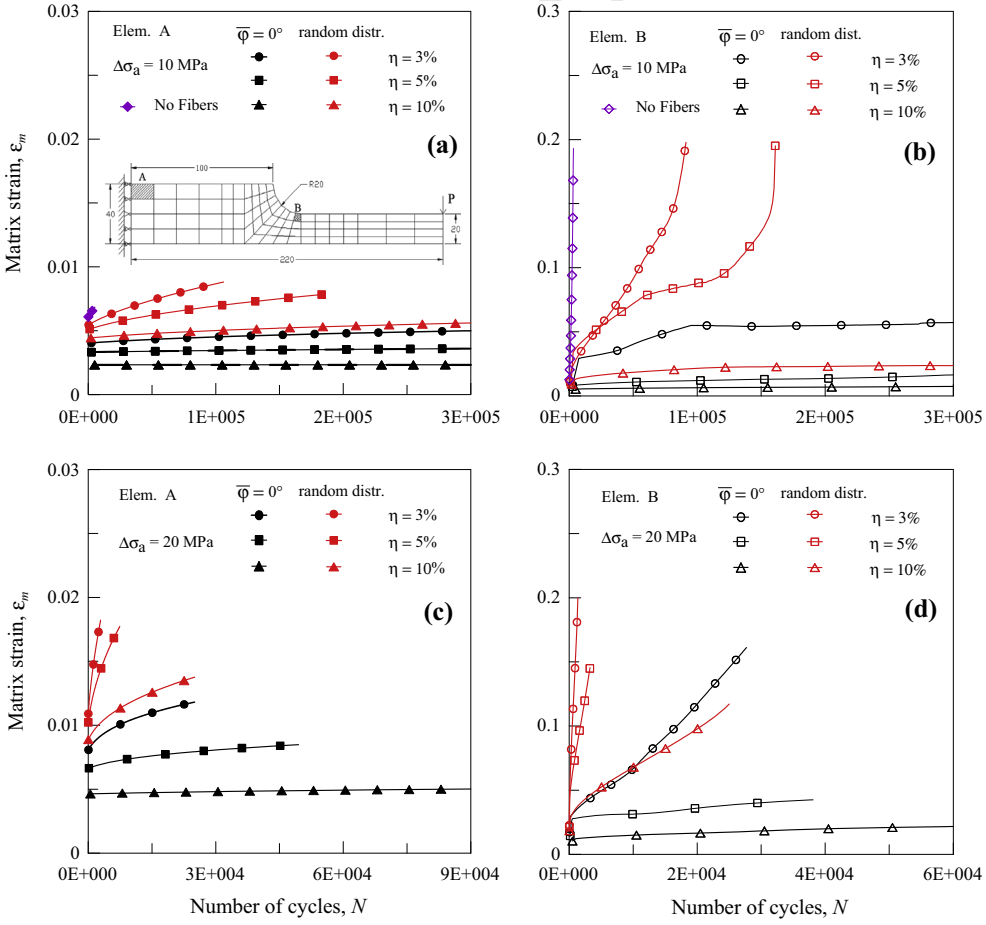

Fig. 7. Matrix strain, ε_m, against number N of loading cycles, related to two elements of the mesh (elem. A (a, c) and elem. B (b, d)), for three fibre volume fractions (η = 3%, 5% and 10%), two fibre orientations ($\bar{\varphi} = 0^\circ$ and randomly distribution) and two values of applied load ($\Delta\sigma_a$ = 10 MPa (a, b) and $\Delta\sigma_a$ = 20 MPa (c, d)). The case of no fibres is also plotted (a, b).

Please cite this article in press as: Brighenti R et al. Micromechanical crack growth-based fatigue damage in fibrous composites. Int J Fatigue (2015), http://dx.doi.org/10.1016/j.ijfatigue.2015.04.007

3.2. FE implementation

The proposed model is implemented in a FE code in order to verify its capability to estimate the fatigue behaviour of fibre-reinforced composites under uniaxial cyclic loading. For the sake of the model applicability in a computational approach, the remotely applied cyclic stresses σ_z^∞ and σ_r^∞ are evaluated at the Gauss points in each finite element, by considering the actual fibre pattern in the composite. In other words, the remote stress field must be decomposed in order to get the axial and radial stresses according to the fibre orientation. In the case of randomly distributed fibres, we have:

$$\sigma_z^\infty = \sigma_r^\infty = \sigma_{ii}/3 \tag{16}$$

and in the case of nearly unidirectional fibres:

$$\sigma_z^\infty = (\mathbf{k}\otimes\mathbf{k}) : \sigma, \qquad \sigma_r^\infty \cong \sigma_{t,ii}/2 \tag{17}$$

where $\sigma_{t,ii}$ are the normal stress tensor components acting in a plane containing the fibre axis identified by the unit vector $\mathbf{k}$.

In the case of fatigue loading, Eq. (10) is employed by considering the interface SIF range (see Eq. (4)) evaluated through the stresses in Eqs. (16) and (17).

In order to numerically evaluate the fibre detachment increment, the whole stress history is subdivided in N_{blocks} blocks, and the fatigue crack growth equation is applied after N_{cycles} of each fatigue block (Fig. 4):

$$\Delta l = N_{cycles} \cdot C_i \cdot \Delta K_i^{m_i} \tag{18}$$

Once the current debonded fibre length is known, the sliding function parameter $s(\varepsilon_f^m) = \varepsilon_f/\varepsilon_f^m$ (given by the ratio of fibre strain to matrix strain measured in the fibre direction [8]) can be evaluated, and the tangent elastic tensor $\mathbf{C}'_{eq}$ of the homogenized material can be obtained:

$$\mathbf{C}'_{eq} = \mu\cdot\mathbf{C}'_m + \eta\cdot E'_f\cdot\left[s(\varepsilon_f^m) + \varepsilon_f^m\cdot\frac{ds(\varepsilon_f^m)}{d\varepsilon_f^m}\right]\cdot\int_\Phi p_\varphi(\varphi)\cdot p_\vartheta(\theta)\cdot\mathbf{F}\otimes\mathbf{F}d\Phi \tag{19}$$

where μ, η are the fibre and matrix volume fractions, respectively, $\mathbf{C}'_m$, E'_f are the tangent elastic tensor of the matrix material and the fibre tangent elastic modulus, respectively, $p_\varphi(\varphi)$ and $p_\vartheta(\theta)$ are the probability distribution functions describing the fibres arrangement in 3D space, and $\mathbf{F}$ is the second-order tensor defined as follows: $\mathbf{F} = \mathbf{k}\otimes\mathbf{k}$.

Such a homogenization procedure is carried out every time the fibre detachment due to fatigue is updated throughout the numerical procedure.

4. Numerical applications

In the present section, the fatigue behaviour of fibre-reinforced composite structural components is analysed. Firstly, two experimental fatigue tests reported in the literature are simulated in

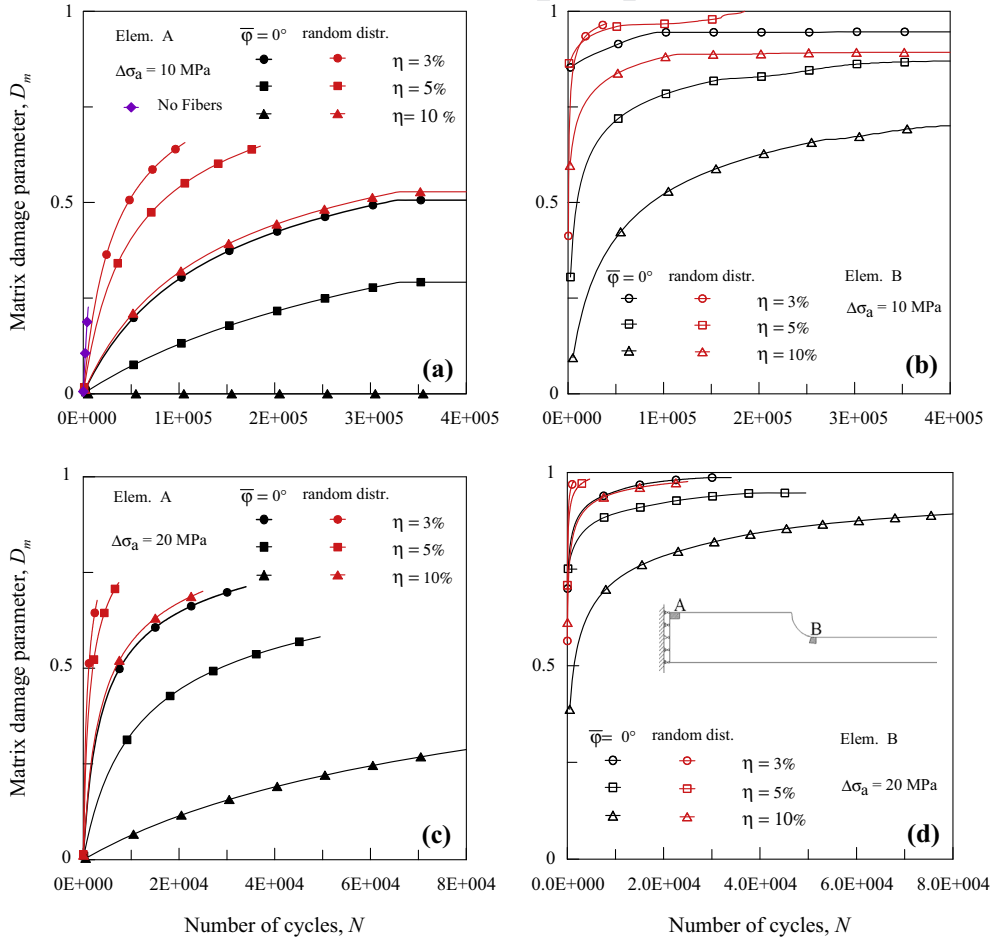

Fig. 8. Matrix damage parameter, D_m, against number of load cycles, N, related to two elements of the mesh (elem. A (a, c) and elem. B (b, d)), for three fibre volume fractions (η = 3%, 5% and 10%), two fibre orientations ($\bar{\varphi} = 0°$ and randomly distribution) and two values of applied load ($\Delta\sigma_a$ = 10 MPa (a, b) and $\Delta\sigma_a$ = 20 MPa (c, d)). The case of no fibres is also plotted (a).

Please cite this article in press as: Brighenti R et al. Micromechanical crack growth-based fatigue damage in fibrous composites. Int J Fatigue (2015), http://dx.doi.org/10.1016/j.ijfatigue.2015.04.007

order to assess the capability of the proposed mechanical model to quantify the fatigue damage in such a class of multiphase materials. The last example examines a fibre-reinforced composite (FRC) structural component with a stress concentrator under cyclic loading, and the fatigue behaviour is determined for different values of the main parameters involved, in order to outline their roles in fatigue problems.

4.1. Fatigue behaviour of a polymeric fibre-reinforced composite

The fatigue behaviour of a 20% glass (randomly distributed) fibre-reinforced polycarbonate specimen under constant amplitude uniaxial cyclic stress is herein examined [21]. The material parameters are as follows: interface Paris constants $C_i = 1.01 \cdot 10^{-4}$, $m_i = 3.1$ (dl/dN in mm/cycle, ΔK_i in MPam; such constants are assumed to be equal to those of the matrix material); Wöhler's constants $\sigma_0 = 5$ MPa, $N_0 \cong 2 \cdot 10^6$, $B = 0.293$; fibre geometry parameters $2L_f = 4 \cdot 10^{-4}$ m, $\phi_f = 10$ μm.

The attainment of the ultimate matrix strain value ($\varepsilon_u = 10\%$) during fatigue cycles is used to identify the fatigue failure condition (Fig. 5a). The dimensionless cyclic stress amplitude σ^*/σ_u ($\sigma_u \cong 75$ MPa is the composite tensile strength) against the number of stress cycles is shown in Fig. 5a, where a good agreement with experimental results can be noticed. Numerical results appear to be approximately aligned along a straight line in the S–N diagram. In Fig. 5b, the damage values are plotted against N for a given value of σ^* in the matrix material and the dimensionless detached length at point P.

4.2. Fatigue behaviour of a polymeric fibre-reinforced composite

In the present example, the fatigue behaviour of a 13% glass fibre-reinforced polyamide specimen (with fibres oriented parallel or inclined of an angle $\varphi = 30^\circ$ with respect to the load direction) under constant amplitude uniaxial cyclic stress is examined [22]. The material parameters are as follows: interface Paris constants $C_i = 8.7 \cdot 10^{-9}$ and $m_i = 13.9$ (dl/dN in mm/cycle, ΔK_i in MPam; such constants are assumed to be equal to those of the matrix material); Wöhler's constants $\sigma_0 = 10$ MPa, $N_0 \cong 2 \cdot 10^6$, $B = 0.133$; fibre geometry parameters $2L_f = 4 \cdot 10^{-4}$ m, $\phi_f = 10$ μm.

In Fig. 6a, the experimental S–N curves for both fibre orientations are reported. As can be noted, the effectiveness of the fibres aligned with the fatigue loading direction is evident and, for the same stress amplitude, a much greater number of stress cycles can be reached before failure.

The numerical simulations of the number of stress cycles to failure confirm the above behaviour, providing results that are in satisfactory agreement with the experimental ones. In Fig. 6b, the damage parameter D_E associated with the Young modulus of the matrix is plotted together with the sliding function against the number N of loading cycles. As can be noted, the function $s(\overline{\varepsilon_f^m})$ decreases with N, indicating a decreasing capability of the fibres to carry the applied load transferred from the matrix. As a consequence, the stress fraction sustained by the matrix increases with N (being constant the maximum applied stress during fatigue process) and, according to Eqs. (13), (14), the damage in the bulk material increases. For the case of fibres aligned with the loading

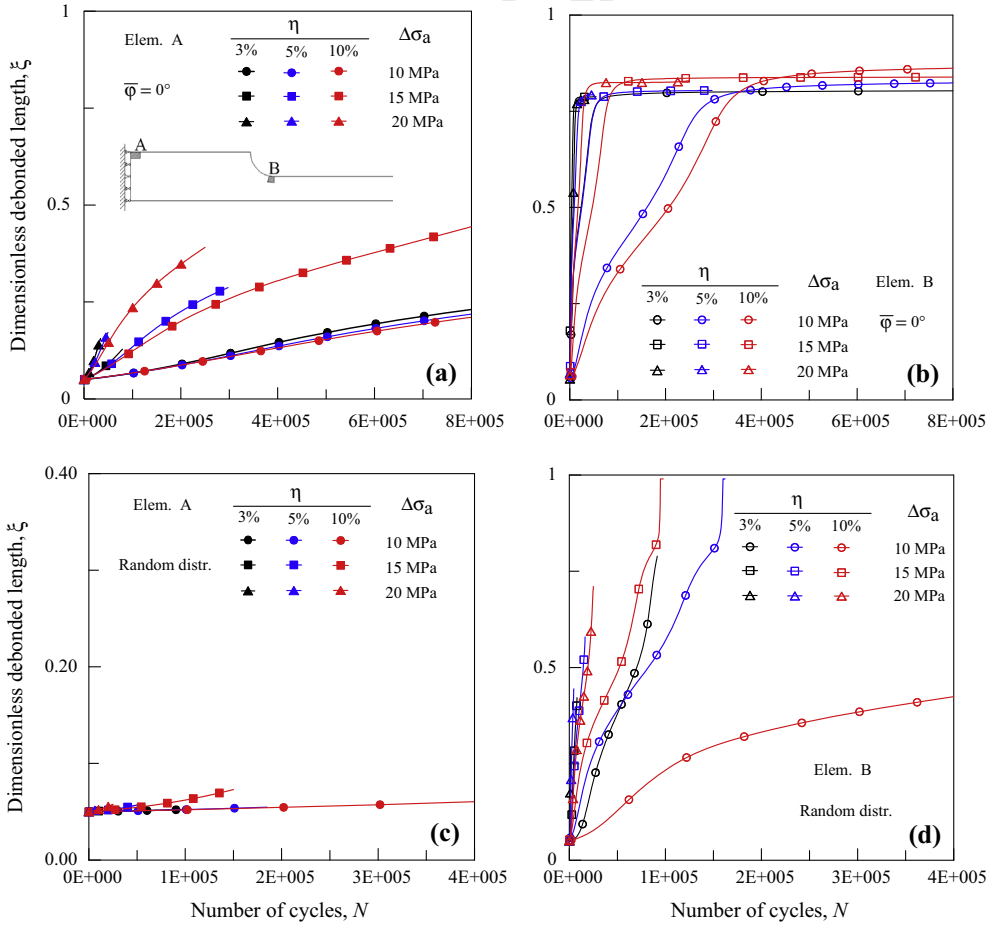

Fig. 9. Dimensionless debonded length, ξ, against number of loading cycles, N, for two elements of the mesh (elem. A (a, c) and elem. B (b, d)), for three fibre volume fractions (η = 3%, 5% and 10%), three values of applied load ($\Delta\sigma_a$ = 10 MPa, 15 MPa and 20 MPa) and two fibre distributions ($\bar{\varphi} = 0^\circ$ (a, b), and randomly arrangement (c, d)).

Please cite this article in press as: Brighenti R et al. Micromechanical crack growth-based fatigue damage in fibrous composites. Int J Fatigue (2015), http://dx.doi.org/10.1016/j.ijfatigue.2015.04.007

direction ($\varphi = 0^\circ$) after a certain number of loading cycles, the sliding parameter stabilises, and the damage in the matrix appears to become very slightly increasing with N.

4.3. Influence of the damage parameters on the fatigue of a composite notched beam

The last parametric example is related to a notched clamped beam under a repeated concentrated load applied to its extremity. Three different fibre contents ($\eta = 3\%, 5\%, 10\%$) and two fibre arrangements ($\bar{\varphi} = 0^\circ$ and random distribution) are analysed. The amplitude of the cyclic stress measured at point A (Fig. 7a) is supposed to be $\Delta\sigma_a = 10, 15, 20$ MPa. For the sake of comparison, the case of a plain material is also examined.The matrix material is characterized by Young modulus $E_m = 2.2$ GPa and Poisson's ratio $\upsilon_f = 0.15$. For the reinforcing fibres with semi-length $2L_f = 4 \cdot 10^{-4}$ m and diameter $\phi_f = 10$ μm, the Young modulus is $E_f = 72.4$ GPa and the Poisson's ratio is $\upsilon_f = 0.3$. The interface fracture energy is assumed to be equal to $G_{ic} = 100$ Nm. The interface Paris constants are $C_i = 1.01 \cdot 10^{-4}$, $m_i = 3.1$ (dl/dN in mm/cycle, ΔK_i in MPam; such constants are assumed to be equal to those of the matrix material) and the Wöhler's constants are $\sigma_0 = 5$ MPa, $N_0 \cong 2 \cdot 10^6$, $B = 0.293$.

Two zones of the beam are examined in order to analyse the cyclic load effects, i.e. an element A close to the boundary constrain and an element B placed at the stress concentration region.

In Fig. 7, the matrix strain evolution against the number of loading cycles is plotted for different fibre arrangements, fibre contents and stress amplitude values. It can be observed that the effectiveness of the fibre phase decreases with N, as is outlined by the increase of the strain in the matrix. An increase of the fibre volume content produces a reduction of the matrix strain; the case of fibres aligned with the horizontal direction seems to be more effective in limiting the matrix strain. The same qualitative behaviour can be recognised for both element A and element B; nevertheless, the increase of the matrix strain in the stress concentration zone (element B) is much more pronounced, especially for low fibre contents.

Fig. 8 shows the damage evolution for the same cases reported in Fig. 7. Since the matrix damage parameter, $D_m = D_E$, is strictly related to the matrix strain, a trend similar to that in Fig. 7 can be observed. It is worth noting that, in the case $\bar{\varphi} = 0^\circ$, $\eta = 10\%$ and $\Delta\sigma_a = 10$ MPa, the damage in the matrix remains zero along the whole fatigue process, and the matrix strain is almost constant.

The fibre dimensionless debonded length against N is plotted in Fig. 9. It is evident that, in the highly stressed element B (Fig. 9b, d), the fibre detachment develops very quickly for both horizontal and randomly oriented fibres, whereas such a behaviour is much more mitigated for element A.

In the case of $\bar{\varphi} = 0^\circ$, the fibre debonding at element B stabilises around the value $\xi \cong 0.8$ for all the considered cases, whereas ξ rapidly tends to the unity for random fibre distribution.

The fibre effectiveness during fatigue process is represented in Fig. 10 through the sliding function s. It is a decreasing function of N, with higher decreasing rate as the stress amplitude increases, the fibre content decreases, the local stress value is high (element

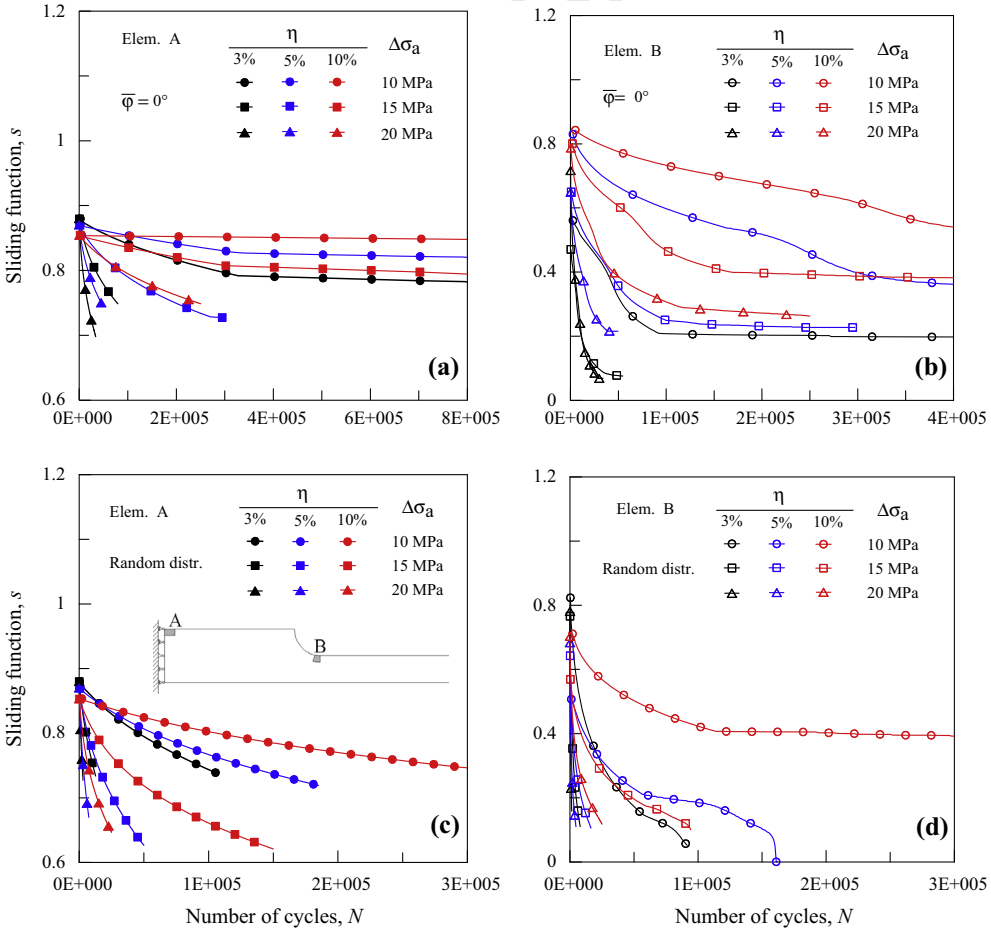

Fig. 10. Sliding function, s, against number of loading cycles, N, related to two elements of the mesh (elem. A (a, c) and elem. B (b, d)) for three fibre volume fractions ($\eta = 3\%$, 5% and 10%), three values of applied load ($\Delta\sigma_a = 10$ MPa, 15 MPa and 20 MPa) and two fibre orientations ($\bar{\varphi} = 0^\circ$ (a, b), and randomly distribution, (c, d)).

Please cite this article in press as: Brighenti R et al. Micromechanical crack growth-based fatigue damage in fibrous composites. Int J Fatigue (2015), http://dx.doi.org/10.1016/j.ijfatigue.2015.04.007

B), and the random distribution is considered instead of the case $\bar{\varphi} = 0°$.

At the beginning of this Section, it has been stated that the fibre–matrix interface parameters used in the numerical calculations are the same as those of the matrix material. The determination of the interface parameters is very difficult [23], and some uncertainties are always unavoidable. For these reasons, the influence of C_i (the Paris law parameter of the interface) is herein examined by varying such a parameter of some orders of magnitude.

In Fig. 11, the damage occurring in the matrix against N is plotted for three values of C_i. Such different values of this parameter are not so important for the damage development since, for a given number of loading cycles, the damage value is approximately independent of C_i. This result is particularly important since it allows us to conclude that the uncertainty in the determination

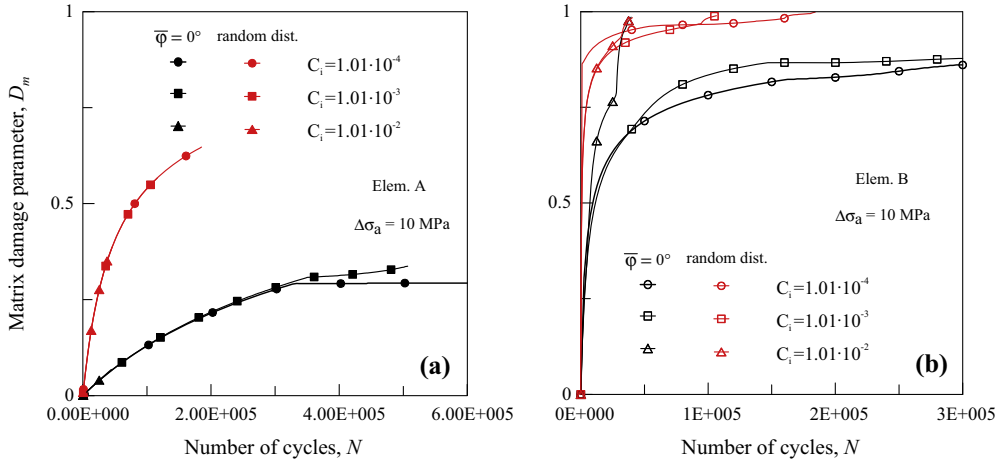

Fig. 11. Matrix damage parameter, D_m, against number of loading cycles, N, related to the elements A (a) and B (b), for η = 5%, two fibre orientations ($\bar{\varphi} = 0°$ and randomly distribution), $\Delta\sigma_a$ = 10 MPa and three different values of the interface fatigue constant, C_i .

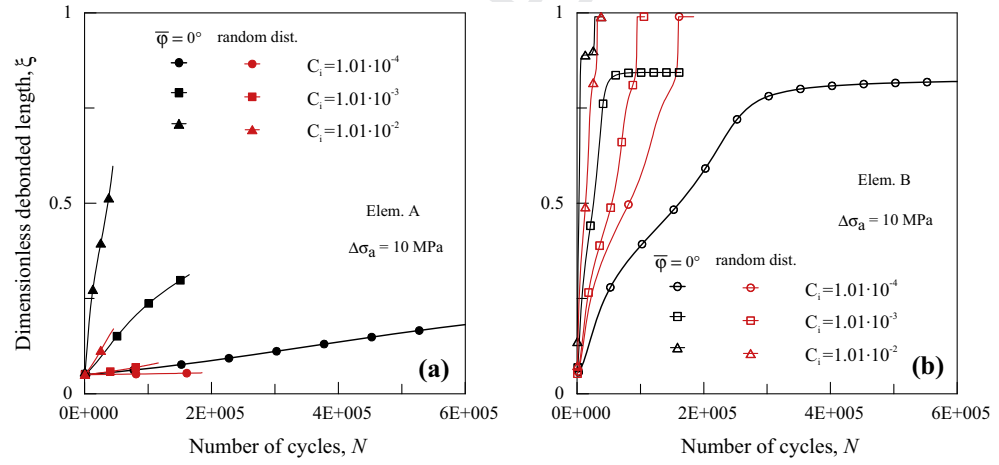

Fig. 12. Dimensionless debonded length, ξ, against number of loading cycles, N, related to the elements A (a) and B (b), for η = 5%, two fibre orientations ($\bar{\varphi} = 0°$ and randomly distribution), $\Delta\sigma_a$ = 10 MPa and three different values of the interface fatigue constant, C_i.

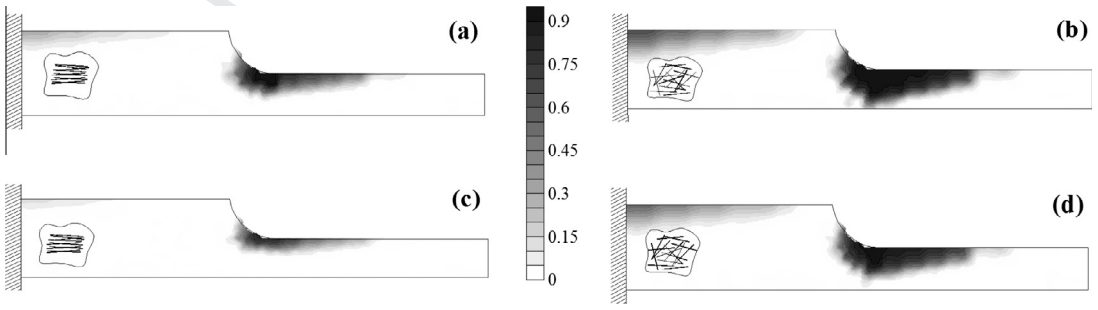

Fig. 13a. Matrix damage parameter, D_m, spatial distribution for η = 3% (a, b) and η = 5% (c, d), two different fibre orientations ($\bar{\varphi} = 0°$ (a, c) and randomly distribution (b, d),) with $\Delta\sigma_a$ = 10 MPa at N = 91,500 cycles.

Please cite this article in press as: Brighenti R et al. Micromechanical crack growth-based fatigue damage in fibrous composites. Int J Fatigue (2015), http://dx.doi.org/10.1016/j.ijfatigue.2015.04.007

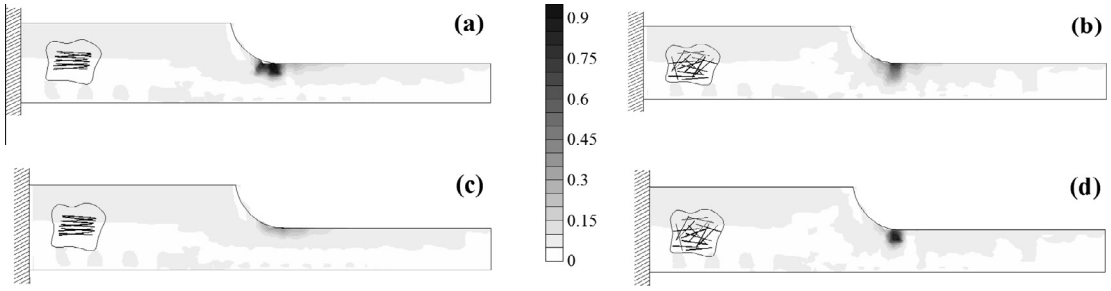

Fig. 13b. Dimensionless debonded length, ξ, spatial distribution for $\eta = 3\%$ (a, b) and $\eta = 5\%$ (c, d), two different fibre orientations ($\bar{\varphi} = 0^{\circ}$ (a, c) and randomly distribution (b, d)), with $\Delta\sigma_a = 10$ MPa at $N = 91{,}500$ cycles.

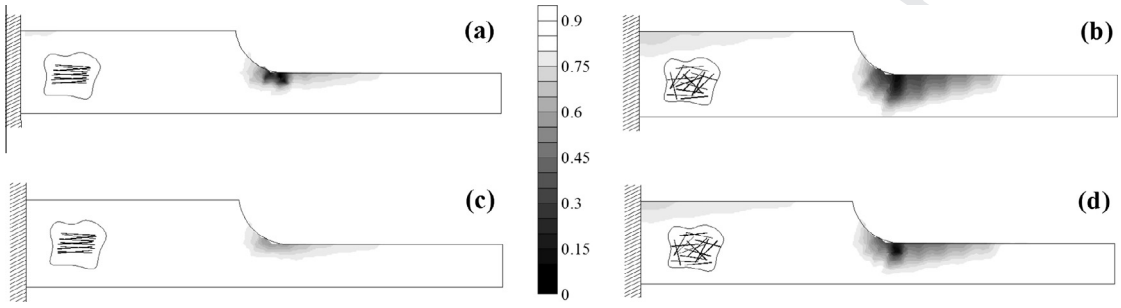

Fig. 13c. Sliding function, s, spatial distribution for $\eta = 3\%$ (a, b) and $\eta = 5\%$ (c, d), two different fibre orientations ($\bar{\varphi} = 0^{\circ}$ (a, c) and randomly distribution (b, d)), with $\Delta\sigma_a = 10$ MPa at $N = 91{,}500$ cycles.

of the fatigue interface parameter has low effects on the matrix damage.

In Fig. 12, the dimensionless fibre detachment ξ against N is plotted for the three values of C_i examined above. The debonding appears to be heavily affected by the value of C_i, especially in zones with low stress values and almost uniform stress distribution (element A). However, such a microscopic quantity (ξ) is not a relevant parameter for the whole behaviour of the composite, while the sliding function represents a suitable parameter of the fibre effectiveness.

By using a grey scale map, Fig. 13a–13c show the distribution of the matrix damage, the fibre dimensionless debonded length, and the sliding function, respectively, for horizontal and randomly distributed fibres and for two values of the fibre content ($\eta = 3\%$ and 5%), at a given number of loading cycles ($N = 91{,}500$) and stress amplitude equal to $\Delta\sigma_a = 10$ MPa.

The case of random fibres corresponds to higher damage in the matrix and lower values of sliding function, denoting the more pronounced efficiency decrease of the reinforcing phase.

Concerning the fibre detached length, a unique trend cannot easily be recognised. The higher amount of fibre content is certainly responsible for a reduction of the fibre debonding that appears to be practically not relevant for $\bar{\varphi} = 0^{\circ}$ and $\eta = 5\%$.

5. Conclusions

A micromechanical model for the fibre–matrix interface damages and matrix degradation due to fatigue loading is proposed in the present paper. In particular, a fracture mechanics-based approach is adopted to describe the fibre debonding, a crack growth rate-based approach is applied to assess the fatigue behaviour of fibre-reinforced composites, and a Wöhler approach is used to quantify the damage in the matrix. An interaction fibre–matrix damage parameter, useful to quantify the debonding severity during fatigue process, is introduced. Finally, some numerical simulation results are compared with literature results, and a parametric example is examined to evaluate the fatigue effects of different mechanical variables and fibre-reinforced conditions on the fatigue behaviour of such materials. The present model, based on the description of the mechanical phenomena taking place at microscopic and mesoscopic level, enables to quantitatively describe the main mechanical detrimental effects produced by repeated loading on fibre-reinforced composites.

References

[1] Jones RMA. Mechanics of composite materials. 2nd ed.. Taylor & Francis Group; 1999.
[2] Mallick PK. Fiber-reinforced composites: materials, manufacturing, and design. 3rd ed. Dekker Mechanical Engineering; 2007.
[3] Cheng QG. Fiber reinforced composites. Hauppauge, NY: Nova Science Publishers Inc; 2012.
[4] Brighenti R. Numerical modelling of the fatigue behaviour of fiber reinforced composites. Comp Part B 2004;35(3):197–210.
[5] Carpinteri A, Spagnoli A, Vantadori S. An elastic-plastic crack bridging model for brittle-matrix fibrous composite beams under cyclic loading. Int J Solids Struct 2006;43:4917–36.
[6] Guo LP, Carpinteri A, Spagnoli A, Sun W. Experimental and numerical investigations on fatigue damage propagation and life prediction of high-performance concrete containing reactive mineral admixtures. J Fat 2010;32:227–37.
[7] Cox HL. The elasticity and strength of paper and other fibrous materials. Br J Appl Phys 1952;3:72–9.
[8] Brighenti R, Scorza D. A micro-mechanical model for statistically unidirectional and randomly distributed fibre-reinforced solids. Mathem Mech Sol 2012;18:876–93.
[9] Brighenti R, Scorza D. Numerical modelling of the fracture behaviour of brittle materials reinforced with unidirectional or randomly distributed fibres. Mech Mater 2012;52:12–27.
[10] Rice JC. Elastic fracture mechanics concepts for interfacial cracks. J Appl Mech 1988;55:98–103.
[11] Hutchinson JW, Mear ME, Rice JC. Crack paralleling an interface between dissimilar materials. J Appl Mech 1987;54:828–32.
[12] Comminou M. The interface crack. J Appl Mech 1977;44:631–6.
[13] Wüthrich C. Stress intensity factors for cylindrical cracks in long cylinders. Engng Fract Mech 1980;13:987–90.
[14] Zbib HM, Hirth JP, Demir I. The stress intensity factor of cylindrical cracks. Int J Engng Sci 1995;33:247–53.

[15] Chaudhuri RA. Three-dimensional singular stress field near a partially debonded cylindrical rigid fibre. Comp Struct 2006;72:141–50.
[16] Brighenti R, Carpinteri A, Scorza D. Fracture mechanics approach for partially debonded cylindrical fibre. Comp Part B 2013;53:169–78.
[17] Brighenti R, Carpinteri A, Scorza D. Stress-intensity factors at the interface edge of a partially detached fibre. Theor Appl Fract Mec 2013;66–67:1–13.
[18] Brighenti R, Carpinteri A, Scorza D. Fatigue crack propagation simulating fibre debonding in cyclically loaded composites. Procedia Material Science (20th European Conference on Fracture ECF20) 2014; 3: 357–62.
[19] Kabir MR, Lutz W, Zhu K, Schmauder S. Fatigue modeling of short fiber reinforced composites with ductile matrix under cyclic loading. Comput Mat Sci 2006;36:361–6.
[20] Brighenti R, Carpinteri A, Corbari N. Damage mechanics and Paris regime in fatigue life assessment of metals. Int J Press Vess Piping 2013;104:57–68.
[21] Zago A. Constant amplitude fatigue of short glass and carbon fiber reinforced thermoplastics. J Reinfor Plastics Compos 2001;20(7):564–95.
[22] Bernasconi A, Davoli P, Basile A, Filippi A. Effect of fibre orientation on the fatigue behaviour on a short glass fibre reinforced polyamide. J Fat 2007;29:199–208.
[23] Soapman MJ, Nazari A, Porter JA, Arola D. A comparison of fatigue crack growth in resin composite, dentin at the interface. Dental Mater 2007;23:608–14.